Neutron transfer reactions induced by ^{8}Li on ^{9}Be

V. Guimarães, R. Lichtenthäler, O. Camargo, and A. Barioni
Instituto de Física, Universidade de São Paulo, P.O. Box 66318, 05389-970 São Paulo, SP, Brazil

M. Assunção
Universidade Federal de Sao Paulo, Campus Diadema, 09941-510 São Paulo, SP, Brazil

J. J. Kolata
Department of Physics, University of Notre Dame, Notre Dame, Indiana, 46556, USA

H. Amro, F. D. Becchetti, and Hao Jiang
Department of Physics, University of Michigan, Ann Arbor, Michigan 48109-1120, USA

E. F. Aguilera, D. Lizcano, E. Martines-Quiroz, and H. Garcia
Instituto Nacional de Investigaciones Nucleares, A. P. 18-1027, C.P. 11801, Distrito Federal, Mexico
(Received 1 November 2006; published 3 May 2007)

Angular distributions for the elastic scattering of ^{8}Li on ^{9}Be and the neutron transfer reactions ^{9}Be(^{8}Li,^{7}Li)^{10}Be and ^{9}Be(^{8}Li,^{9}Li)^{8}Be were measured with a 27 MeV ^{8}Li radioactive nuclear beam. Spectroscopic factors for $^{8}\text{Li} \otimes \text{n} = {}^{9}\text{Li}$ and $^{7}\text{Li} \otimes \text{n} = {}^{8}\text{Li}$ bound systems were obtained from the comparison between the experimental differential cross section and finite-range distorted-wave Born approximation calculations with the code FRESCO. The spectroscopic factors obtained were compared to shell model calculations and to other experimental values from (d,p) reactions. Using the present values for the spectroscopic factor, cross sections for the direct neutron-capture reactions ^{7}Li(n,γ)^{8}Li and ^{8}Li(n,γ)^{9}Li were calculated in the framework of a potential model.

DOI: 10.1103/PhysRevC.75.054602 PACS number(s): 21.10.Jx, 25.60.Je, 25.40.Lw

I. INTRODUCTION

Spectroscopic study of nuclei far from the valley of β stability is one of the major active fields in nuclear physics. To perform nuclear spectroscopic investigation on such nuclei, direct reaction processes that add or remove one or a few nucleons, such as direct stripping and pickup reactions, from which one can identify single-particle orbitals, energies, and their occupancies, are commonly used. With the improvement of radioactive ion beam intensities it is now possible to obtain reliable measurements of transfer cross sections induced by unstable projectiles, and together with finite-range computer codes such as FRESCO [1], it becomes possible to obtain spectroscopic information on unstable nuclei with good precision.

In particular, spectroscopic investigation of unstable lithium isotopes is of interest not only for understanding nuclear structure and reaction mechanisms, where spectroscopic factors of these isotopes can be an important experimental probe for single-particle dynamics, shell model calculations, and halo properties [2–5], but also for astrophysics. In the inhomogeneous nucleosynthesis models [6], reactions with ^{8}Li can bridge the $A = 8$ mass gap and heavier elements can then be synthesized in the early universe. It also has been pointed out that neutron-induced three-particle interactions can be important in a high neutron abundance environment [7]. In this case, heavier elements would be synthesized via the reaction sequence ^{4}He(2n,γ)^{6}He(2n,γ)^{8}He(β^{+})^{8}Li. Here again, ^{8}Li plays an important role in the subsequent synthesis of heavier elements. Likewise, light neutron-rich nuclei such as ^{8}Li have been found to be important to produce seed nuclei for the r-process, e.g., in Type II supernovae [8].

Once ^{8}Li is produced two possible competing chains of reactions can take place: ^{8}Li(α,n)^{11}B(n,γ)^{12}B(β^{+})^{12}C and ^{8}Li(n,γ)^{9}Li(α,n)^{12}B(β^{+})^{12}C. The key reaction for the second chain is ^{8}Li(n,γ)^{9}Li. Direct measurement of this reaction is impossible because no neutron target exists and the half-life of ^{8}Li is too short (838 ms) for ^{8}Li to be used as a target. Thus, experimental information on the cross section for this reaction must be obtained by some indirect methods. Kobayashi *et al.* [9] used the Coulomb dissociation method, which is the inverse of the capture process. However, in this work only an upper limit for the cross section at low energy was obtained. Another indirect approach that may be used to investigate capture reactions is the ANC (asymptotic normalization coefficient) method, where the (d,p) reaction in inverse kinematics is used to extract an "asymptotic normalization coefficient" that can be related to the capture cross section. The ANC is obtained from peripheral transfer reactions whose amplitudes contain the same overlap function as the amplitude of the corresponding capture reaction of interest [10] and therefore can be used to normalize the nonresonant part of the capture reaction. The method is based on the assumption that capture reactions at stellar energies usually proceed through the tail of the nuclear overlap function. The amplitude of the radiative capture cross section is then dominated by contributions from large relative distances of the participating nuclei. However, it has been shown that *s*-wave neutron

capture, even at rather low energies, is not peripheral [11,12] and so it is necessary to use a potential model to calculate the wave function of the incoming neutron in this case. This indirect approach, based on the potential model, has been recently applied in the analysis of the ^{16}O(d,p)^{17}O and ^{16}O(d,n)^{17}F transfer reactions to determine the corresponding ^{16}O(p,γ)^{17}F and ^{16}O(n,γ)^{17}O astrophysical direct capture cross sections [13].

Early measurements of neutron transfer reactions induced by stable lithium isotopes on a ^{9}Be target (^{9}Be(^{7}Li,^{6}Li)^{10}Be [14] and ^{9}Be(^{6}Li,^{7}Li)^{8}Be [15]) have shown that these reactions are good tools for obtaining spectroscopic information. In this article, we report on the measurement and analysis of angular distributions for two neutron transfer reactions induced by a radioactive ^{8}Li beam: ^{9}Be(^{8}Li,^{9}Li)^{8}Be and ^{9}Be(^{8}Li,^{7}Li)^{10}Be. From a finite-range distorted-wave Born approximation (FR-DWBA) analysis of these angular distributions, the spectroscopic factors for the $^{7}\mathrm{Li}_{gs} \otimes \mathrm{n} = {}^{8}\mathrm{Li}_{gs}$ and $^{8}\mathrm{Li}_{gs} \otimes \mathrm{n} = {}^{9}\mathrm{Li}_{gs}$ bound systems were extracted, and cross sections and nucleosynthesis reaction rates for the nonresonant part of the ^{7}Li(n,γ)^{8}Li and ^{8}Li(n,γ)^{9}Li capture reactions were derived.

II. THE EXPERIMENT

Angular distributions for ^{8}Li elastic scattering and the ^{9}Be(^{8}Li,^{9}Li)^{8}Be and ^{9}Be(^{8}Li,^{7}Li)^{10}Be neutron transfer reactions have been measured at the Nuclear Structure Laboratory of the University of Notre Dame, USA. The 27 MeV secondary ^{8}Li radioactive beam was obtained from the *TwinSol* RNB system [16]. In this system, the beam was produced in a primary target via the ^{9}Be(^{7}Li,^{8}Li) reaction, where a 30 MeV primary ^{7}Li beam having an intensity of up to 1 eμA was obtained from a 9.5 MV tandem Van de Graaff accelerator. The production target consisted of a beryllium foil 12 μm thick mounted as the exit window of a gas cell that was filled with ^{4}He gas at a pressure of 1 atm for cooling purposes (the entrance window of the gas cell consisted of a 2 μm thick Havar foil). The two superconducting solenoids in the *TwinSol* system act as thick lenses to collect, select, and focus the secondary beam into a scattering chamber. The 27 MeV ^{8}Li beam had an average intensity of 5.0×10^{5} particles per second per 1 eμA of primary beam and an energy resolution of 0.450 MeV (FWHM) determined from the elastic scattering measurement on a gold target. The beam was focused onto a 1.44 mg/cm^2 thick ^{9}Be secondary target. Some beam contaminants (^{4}He, ^{6}He, and ^{7}Li) with the same magnetic rigidity as ^{8}Li were also present but did not produce reaction products with mass $A = 8$ or $A = 9$ in the same range of energy as the particles from the neutron transfer reactions of interest.

The scattered ^{8}Li particles and ^{7}Li and ^{9}Li reaction products were detected by an array of ΔE-E Si telescopes. The measurements were performed with two setups, where a combination of the three telescopes covered the range of laboratory angles from 15 to 40 degrees. An overlap of angles in these setups was useful for normalization purposes. The telescopes consisted of 20- to 25-μm Si ΔE detectors backed by 300 μm thick Si E detectors. The detector telescopes had circular apertures that subtended a solid angle of 4×10^{-3} sr for the most forward-angle measurements and 8–15 $\times 10^{-3}$ sr for the backward angles. A collimator placed in front of the first solenoid limited the angular acceptance of the particles produced in the primary target to the range of 2.5°–6.0°. This introduces an angular divergence in the secondary beam of about $\pm 3°$. Because the angular aperture of the collimators in front of the detectors was also about $\pm 3°$, the average detection angle was determined by a Monte Carlo simulation, which took into account the collimator size in front of the detectors, the secondary beam spot size on the secondary target (4 mm), the secondary beam divergence, and the angular distribution in the range of the detector aperture (Rutherford on gold and calculated in an iterative way for the ^{9}Be target).

The simultaneous measurement of the transfer products and elastic scattering was very useful to check the consistency of the overall normalization and to select an optimal set of optical model potential parameters. The latter are very important in the FR-DWBA transfer calculations. During the experiment ^{8}Li elastic scattering on a gold target, which was pure Rutherford, was also measured to obtain the absolute normalization of the data.

III. DATA ANALYSIS

Reaction products were identified using a two-dimensional $[C(Z, M) \times E_{\mathrm{total}}]$ plot. The particle identification constant $C(Z, M)$ is given by $C(Z, M) = (E_{\mathrm{total}})^{b} - (E_{\mathrm{total}} - \Delta E)^{b}$ [17], where $E_{\mathrm{total}} = \Delta E + E_{\mathrm{residual}}$ and $b = 1.70$ for these light particles. This constant appears as straight lines as a function of the energy for each Z and M particle in the two-dimensional spectrum $[C(Z, M) \times E_{\mathrm{total}}]$. A typical particle identification spectrum is shown in Fig. 1 for the lithium and helium isotope region. In this plot the ^{8}Li scattered beam particles and the ^{9}Li and ^{7}Li reaction products are shown and can be easily identified.

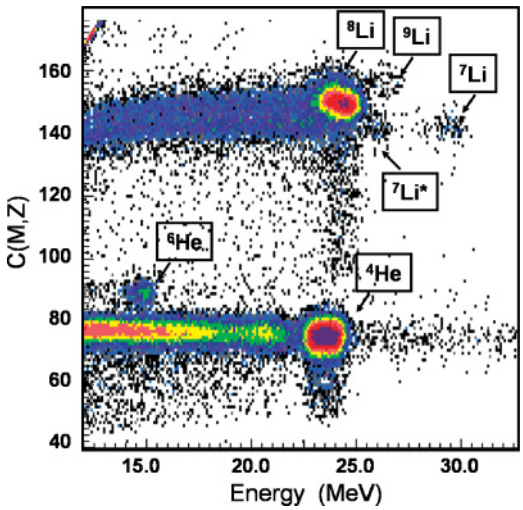

FIG. 1. (Color online) Typical particle identification spectrum $[C(Z, M) \times E_{\mathrm{total}}]$ showing the lithium and helium isotope region for the interaction of ^{8}Li + ^{9}Be at 15 degrees. The elastic scattering (^{8}Li) and reaction products (^{7}Li and ^{9}Li) are indicated, as well as the ^{4}He and ^{6}He contamination in the secondary beam.

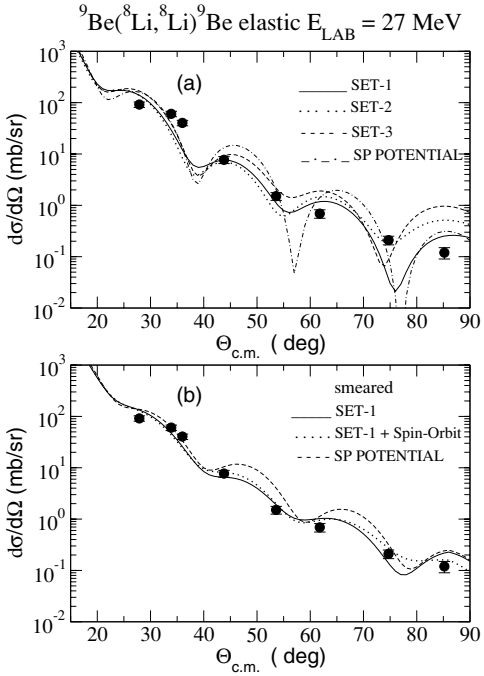

FIG. 2. The differential cross sections for elastic scattering (^{9}Be(^{8}Li,^{8}Li)^{9}Be) at 27 MeV incident ^{8}Li laboratory energy. The curves are optical model calculations with the sets of parameters listed in Table I. The curves in Panel (b) are smeared out by the angular resolution.

A. Elastic scattering

The ^{8}Li energy spectra were obtained by selecting and projecting the ^{8}Li region in the $[C(M, Z) \times E_{\text{total}}]$ plot. The experimental resolution, 0.450 MeV (FWHM), was sufficient to separate elastic scattering from inelastic scattering to the first excited state of ^{8}Li ($E_x = 0.980$ MeV). The experimental angular distribution obtained for the elastic scattering of ^{8}Li on ^{9}Be is shown in Fig. 2. The data were analyzed with the optical model (OM) using volume-type Woods-Saxon nuclear potentials and Coulomb potentials due to uniform charged spheres. The optical parameters used to describe the ^{9}Be(^{8}Li,^{8}Li) elastic scattering are from Refs. [14] and [18] and are listed in Table I. The results of the OM calculations using these potential parameters can be seen in Fig. 2. The OM calculations show more oscillations than the elastic scattering data. In Fig. 2(b) we show the calculated angular distributions smeared by the range of the angular aperture and beam angular dispersion ($\Delta\Theta = 10^{\circ}$ in the c.m.). As one can see, the comparison with the data is improved by smearing the calculated angular distributions. The curve indicated as the SP Potential corresponds to OM calculations using the Sao Paulo Potential [19], which is a double-folding potential with energy dependence and nonlocality correction. Including a spin-orbit term, $V_{\text{SO}} = 7.0$ MeV, in the optical potential did not change the results. Although there was no attempt to adjust the parameters to fit the data, the calculations with all of these potentials give a good description of the elastic scattering data. The SP Potential also reproduces quite well the absolute normalization, which is of some interest considering that this folding-model potential has no free parameters.

These potentials were used in the DWBA calculations for the transfer reactions as described in the following sections.

B. Neutron stripping reaction: ^{9}Be(^{8}Li,^{7}Li)^{10}Be

The ^{9}Be(^{8}Li,^{7} Li$_{\text{gs}}$)^{10}Be$_{\text{gs}}$ reaction has a positive Q value of +4.780 MeV. Thus, the ^{7}Li particles from this transfer reaction could easily be separated from the elastic ^{8}Li particles in the $C(M, Z) \times$ Energy plot. At the most forward angles (15 and 18 degrees) the ^{7}Li group was double peaked because of inelastic scattering to the first excited state of ^{7}Li* at $E_x =$ 0.470 MeV. Although the overall experimental energy resolution (0.450 MeV) was barely sufficient to resolve the ^{7}Li g.s. from the first excited state, it appears that (^{8}Li,^{7}Li$_{\text{gs}}$) was the dominant neutron transfer mode. At backward angles, the ^{7}Li groups observed were centered at the g.s. energies and were not double peaked, at least within the statistics obtained. At the most forward angles, the second excited state of ^{7}Li ($E_x = 2.70$ MeV) was also observed but is not considered in the present analysis. The angular distribution for the ^{9}Be(^{8}Li,^{7} Li$_{\text{gs}}$)^{10}Be$_{\text{gs}}$ reaction is shown in Fig. 3. As can be seen, the differential cross sections for this transfer process are not very large (less than 1 mb/sr) which made the measurements quite difficult at the backward angles because of the limited secondary beam intensity.

FR-DWBA calculations for the ^{9}Be(^{8}Li,^{7}Li) neutron transfer reaction have been performed using the code FRESCO [1]. For each FR-DWBA calculation, the same optical model potential parameters (Table I) were used for both entrance (^{8}Li + ^{9}Be) and exit (^{7}Li + ^{10}Be) channels. The bound-state wave functions were generated with Woods-Saxon potentials and geometric parameters $r = 1.25$ fm and $a = 0.65$ fm, with the depths of the potentials adjusted to give the correct separation energies. In the present (^{8}Li,^{7}Li) DWBA calculation the neutron is considered to be transferred from the $p_{3/2}$ orbital in ^{8}Li$_{\text{gs}}$($J^{\pi} = 2^{+}$) to the $p_{3/2}$ orbital in ^{10}Be$_{\text{gs}}$($J^{\pi} = 0^{+}$), leaving ^{7}Li in its g.s. $J^{\pi} = \frac{3}{2}^{-}$. However, the contribution

TABLE I. Optical model potential parameters. Radii are given by $R_x = r_x \times A_T^{1/3}$.

Set	V^{a}(MeV)	r_R (fm)	a_R (fm)	$W_V{}^{a}$ (MeV)	r_I (fm)	a_I (fm)	r_C (fm)	References
1	173.1	1.19	0.78	8.90	2.52	0.924	1.78	^{7}Li + ^{9}Be at 34 MeV [14]
2	234.4	1.21	0.76	8.90	2.43	1.020	1.78	^{7}Li + ^{9}Be at 34 MeV [14]
3	152.0	1.38	0.75	6.72	2.72	0.900	1.20	^{7}Li + ^{9}Be at 24 MeV [18]

[a]Volume Woods-Saxon potential.

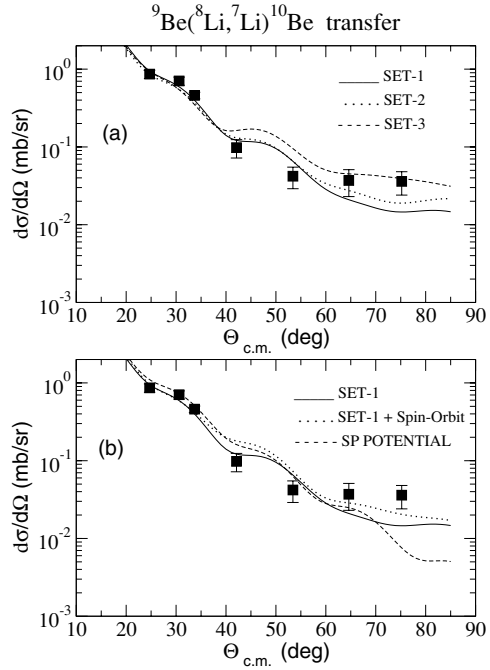

FIG. 3. The differential cross sections for the ^{9}Be(^{8}Li, ^{7}Li$_{gs}$)^{10}Be$_{gs}$ neutron transfer reaction at 27 MeV incident energy. The curves are FR-DWBA calculations using the code FRESCO with the potentials indicated (see Table I), as discussed in the text. The curves are smeared out by the angular resolution.

of the $p_{1/2}$ orbital admixture in the ^{8}Li g.s. is found to be 13% of that $p_{3/2}$ [20]. In the FR-DWBA calculation for the ^{9}Be(^{8}Li,^{7}Li$_{gs}$)^{10}Be$_{gs}$ neutron transfer reaction, the spectroscopic factors from the two vertices must be taken into account. For the ^{9}Be$_{gs} \otimes$ n $= {}^{10}$Be$_{gs}$ vertex, the spectroscopic factor was taken to be $S_{^{10}\mathrm{Be}} = 2.23 \pm 0.13$, which is the average of values from two (d,p) studies [21,22]. The spectroscopic factor for the other ^{7}Li$_{gs} \otimes$ n $= {}^8$Li$_{gs}$ vertex has two contributions, one from the neutron transfer to the $p_{3/2}$ orbital in ^{8}Li(gs), which was taken as $S_{^8\mathrm{Li}}(\mathrm{gs})(3/2) = 0.87$ from Ref. [12] and the other contribution is from the transfer to the $p_{1/2}$ orbital in ^{8}Li(gs) taken as $S_{^8\mathrm{Li}}(\mathrm{gs})(1/2) = 0.113$, which is 13% of that for the $p_{3/2}$ according to Ref. [20]. These values are listed in Table II. As one can see from this table, the experimental values are compatible with the Cohen and Kurath shell model calculation [23]. A similar situation has been found in the analysis of the ^{9}Be(^{7}Li,^{6}Li)^{10}Be [14] and ^{9}Be(^{6}Li,^{7}Li)^{8}Be reactions [15], where the spectroscopic factor for both vertices involved in the transfer agreed with values calculated by Cohen and Kurath. These results indicate that Cohen-Kurath wave functions describe stable lithium and beryllium isotopes in the mass range $A = 6$ to $A = 10$ reasonably well.

C. Neutron pick-up: ^{9}Be(^{8}Li,^{9}Li)^{8}Be

The ^{9}Be(^{8}Li,^{9}Li)^{8}Be neutron transfer reaction can proceed by two possible contributions that leave ^{9}Li in its g.s. These correspond to neutron transfer to either a $1p_{1/2}$ or $1p_{3/2}$ orbit in ^{9}Li. Here only transfer to the $1p_{3/2}$ orbit is considered because the contribution of the $1p_{1/2}$ orbit has been found to be less than 5% [24]. FR-DWBA calculations for the ^{9}Be(^{8}Li,^{9}Li) neutron transfer reaction have been performed using also the code FRESCO [1]. For each FR-DWBA calculation, the same optical model potential parameters (Table I) were used for both entrance (^{8}Li + ^{9}Be) and exit (^{9}Li + ^{8}Be) channels. The bound-state wave functions were generated with Woods-Saxon potentials and geometric parameters $r = 1.25$ fm and $a = 0.65$ fm, with the depths of the potentials adjusted to give the correct separation energies. To obtain the spectroscopic factor for the ^{8}Li$_{gs} \otimes$ n $= {}^9$Li$_{gs}$ vertex, the spectroscopic factor for ^{8}Be$_{gs} \otimes$ n $= {}^9$Be$_{gs}$ must be known. A value of $S_{^9\mathrm{Be}} = 0.44(7)$ was used for this vertex, which is the average of spectroscopic factors from two (d,t) reactions [22,25]. This is somewhat smaller than the Cohen-Kurath prediction (see Table II). Normalizing the FR-DWBA calculation to the experimental data, a spectroscopic factor of $S_{^9\mathrm{Li}} = 0.62 \pm 0.13$ was obtained for the ^{8}Li$_{gs} \otimes$ n $= {}^9$Li$_{gs}$ bound system. The results of the FR-DWBA calculations with different sets of parameters are

TABLE II. Spectroscopic factors C^2S.

	J^π	Shell model calculation	(d,p)	(d,t)	This work Sets 1–3
^{8}Li$_{gs} \otimes$ n $= {}^9$Li$_{gs}$	3/2−	0.628[a] 0.885[b]	0.68(14)[d] 0.90[e]		0.62 (13)
^{7}Li$_{gs} \otimes$ n $= {}^8$Li$_{gs}(p_{3/2})$	2+	0.977[c]	0.87[f]		0.87 (15)
^{7}Li$_{gs} \otimes$ n $= {}^8$Li$_{gs}(p_{1/2})$	2+	0.0561[c]	0.113[g]		0.113 (17)
^{8}Be$_{gs} \otimes$ n $= {}^9$Be$_{gs}$	3/2−	0.580[c]		0.44(7)[i]	
^{9}Be$_{gs} \otimes$ n $= {}^{10}$Be$_{gs}$	0+	2.357[c]	2.23 (13)[h]		

[a]From Ref. [4].
[b]From Ref. [27] using same Cohen Kurath wave-function.
[c]From Cohen and Kurath [23].
[d]From (d,p) reaction at 39 MeV [26].
[e]From (d,p) reaction at 76 MeV [28].
[f]From Ref. [12].
[g]From Ref. [20].
[h]Average of $S = 2.10$ from Ref. [22] and $S = 2.356$ from Ref. [21].
[i]Average of $S = 0.37$ from Ref. [22] and $S = 0.51$ from Ref. [25].

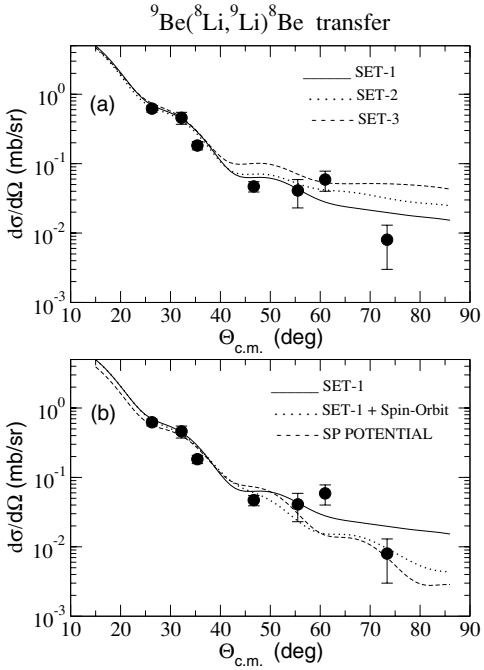

FIG. 4. The differential cross sections for the ^{9}Be(^{8}Li,^{9}Li$_{gs}$)^{8}Be$_{gs}$ neutron transfer reaction at 27 MeV incident energy. The curves are FR-DWBA calculations using the code FRESCO with the potentials indicated, as discussed in the text. The curves are smeared out by the angular resolution.

shown in Fig. 4. As one can see, the calculations agree extremely well with the data at forward angles. The uncertainty in the spectroscopic factor is estimated to be about 20% because of the uncertainties in the experimental data at forward angles and in the spectroscopic factor for the $^{8}\mathrm{Be}_{gs} \otimes \mathrm{n} = {}^{9}\mathrm{Be}_{gs}$ vertex.

The spectroscopic factor obtained for the $^{8}\mathrm{Li}_{gs} \otimes \mathrm{n} = {}^{9}\mathrm{Li}_{gs}$ system in the present analysis is compared with other experimental values and shell model calculations in Table II. Our result agrees very well with the value from the shell model calculation of Ref. [4] and with the experimental value obtained from a (d,p) reaction at lower energy [26], but is lower than the values obtained from a recent calculation using Cohen and Kurath wave functions [27] and from a (d,p) reaction study at higher energy [28]. An analysis with the SP folding-model potential was also performed and spectroscopic factors $S_{^{8}\mathrm{Li}} = 0.68$ and $S_{^{9}\mathrm{Li}} = 0.40$ were obtained. These values are about 35% lower than those obtained with Sets 1, 2, and 3 for both the (^{8}Li,^{7}Li) and (^{8}Li,^{9}Li) transfer reactions. This may be related to nonlocality effects that are taken into account in the folding-model potential but not in the optical model potentials. Further investigation of this subject appears to be warranted.

To extract the spectroscopic factors from the present transfer angular distributions, only the angular range $\theta_{\mathrm{c.m.}} \leqslant 45$ degrees was considered. To verify the peripherality of this transfer reaction, the influence of the internal part of the overlap function was tested in the DWBA calculation. The result of such a test can be seen in Fig. 5. Increasing the radius cut in the radial integral up to $R_{\mathrm{cut}} = 4.0$ fm did

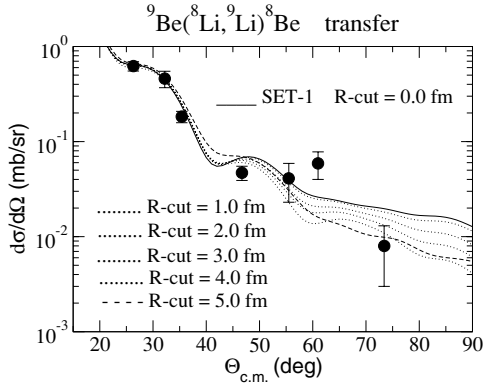

FIG. 5. Angular distribution for the ^{9}Be(^{8}Li,^{9}Li$_{gs}$)^{8}Be$_{gs}$ neutron transfer reaction at 27 MeV incident energy. The solid line corresponds to the FR-DWBA calculation with potential Set 1 (Table I). The dotted lines are FR-DWBA calculations with cutoffs in the radial form factor integral as indicated. The dashed curve is the FR-DWBA calculation with a cutoff radius of 5.0 fm.

not produce any change in the FR-DWBA calculation in the angular range from 0 to 45 degrees. Only for $R_{\mathrm{cut}} > 5.0$ fm, which corresponds to a radius larger than the distance of closest approach of the two interacting nuclei (i.e., $R = 1.25 \times (A_1^{1/3} + A_2^{1/3})$ fm), is the calculation sensitive to the radius cut, as observed in the change of the trend in the curve for $R_{\mathrm{cut}} = 5.0$ fm as compared with the other curves in Fig. 5. Thus, we conclude that indeed this transfer reaction is peripheral at the angles and energy considered here.

IV. RADIATIVE NEUTRON CAPTURE REACTIONS

To calculate the ^{7}Li(n,γ)^{8}Li and ^{8}Li(n,γ)^{9}Li radiative capture reaction cross sections, the computer code RADCAP [29], based on a potential model, was used. In the potential model framework, the direct neutron radiative capture by a nucleus b going to a composite nucleus c via a transition with $E1$ electric dipole character is given by

$$\sigma^{E1}_{b\to c}(n,\gamma) = \frac{16\pi}{9\hbar} k_\gamma^3 \left| Q^{E1}_{b\to c} \right|^2, \tag{1}$$

where $k_\gamma = \epsilon_\gamma/\hbar c$ is the wave number corresponding to a γ-ray energy, ϵ_γ. The term $Q^{E1}_{b\to c}$ is the $E1$ transition matrix element given by

$$Q^{E1}_{b\to c} = \langle \psi_{\mathrm{scat}} | O^{E1} | I_{\mathrm{bound}} \rangle, \tag{2}$$

where O^{E1} stands for the electric dipole operator and the initial-state wave function ψ_{scat} is the incoming neutron wave function scattered by the neutron-nucleus potential. Here the effective charge for the neutrons used in the electric dipole operator is given by $e_{\mathrm{eff}} = -eZ/A$, where A is the mass of the compound nucleus. The wave functions necessary in the potential model are obtained by solving the scattering and bound-state systems, respectively, for a given potential. Thus, the essential ingredients of the model are the potentials used to generate the wave functions ψ_{scat} and I_{bound} and the normalization for the latter which is given by the spectroscopic factor.

A. The ^{7}Li(n,γ)^{8}Li capture reaction

The direct radiative capture (DRC) of a s- or d-wave neutron by ^{7}Li, leaving the ^{8}Li compound nucleus in either the g.s. ($J^\pi = 2^+$) or the first excited state($J^\pi = 1^+$, $E_x =$ 0.980 MeV) proceeds by an $E1$ transition. To calculate the capture cross section in the potential model, a Woods-Saxon form with radius and diffuseness parameters $r_0 = 1.25$ fm and $d = 0.65$ fm, respectively, was adopted for both bound-state and scattering potentials. The depth of the bound-state potentials, $V_0(\text{gs}) = 46.38$ MeV and $V_0(1\text{st}) = 43.30$ MeV, were adjusted to reproduce the corresponding binding energies ($E_{\text{gs}} = 2.033$ MeV and $E_{1\text{st}} = 1.052$ MeV) of the ^{8}Li g.s. and first excited state, respectively. The potentials used to describe the scattering of the neutron by the ^{7}Li nucleus also had geometric parameters $r_0 = 1.25$ fm and $d = 0.65$ fm. Well depths of $V_0 = 56.15$ MeV and $V_0 = 46.50$ MeV were used for the two channel-spin components $s = 2$ and $s = 1$, respectively. These potentials were obtained by Nagai *et al.* [12] by adjusting the well depths to reproduce the experimental n + ^{7}Li scattering lengths ($a_+ = -3.63$ and $a_- = +0.87$) of the two channel-spin components. To calculate the cross sections for the ^{7}Li(n,γ)^{8}Li capture reaction, leaving ^{8}Li in the g.s. ($J^\pi = 2^+$) and first excited state ($J^\pi = 1^+$), we used the same potential parameters for the scattering potentials and the same spectroscopic factors (i.e., $S_{^8\text{Li}}(\text{gs}) = 0.87$ and $S_{^8\text{Li}}(1\text{st}) = 0.48$ for the $^7\text{Li}_{\text{gs}} \otimes \text{n} = {}^8\text{Li}_{\text{gs}}$ and $^7\text{Li}_{\text{gs}} \otimes \text{n} = {}^8\text{Li}_{1\text{st}}$, respectively) as obtained by Nagai *et al.* [12]. The results of this calculation, assuming only an s-wave neutron capture, are compared in Fig. 6 with the experimental data from Refs. [12,30–32], and [33]. The s-wave direct neutron capture contribution is the dominant process, and the contribution from the d-wave neutron is found to be negligible (less than 0.5%) at these low energies. The upper solid curve in Fig. 6 was obtained by using the spectroscopic factor $S_{^8\text{Li}}(\text{gs}) = 1.03\,(15)$ for the $^7\text{Li}_{\text{gs}} \otimes \text{n} = {}^8\text{Li}_{\text{gs}}$ bound state obtained from the present analysis of the ^{9}Be(^{8}Li,^{7}Li) transfer reaction. The different potentials used for the two different couplings of the entrance channel spin were crucial in the calculation to correctly describe the known data. As can be seen, this produces a better agreement of the calculation with the low-energy data. Once we verified that the procedure to obtain the parameters used in the potential model calculation reproduced the experimentally known cross section for the ^{7}Li(n,γ)^{8}Li capture reaction, we then extended this procedure to calculate the cross section for the ^{8}Li(n,γ)$^9\text{Li}_{\text{gs}}$ capture reaction.

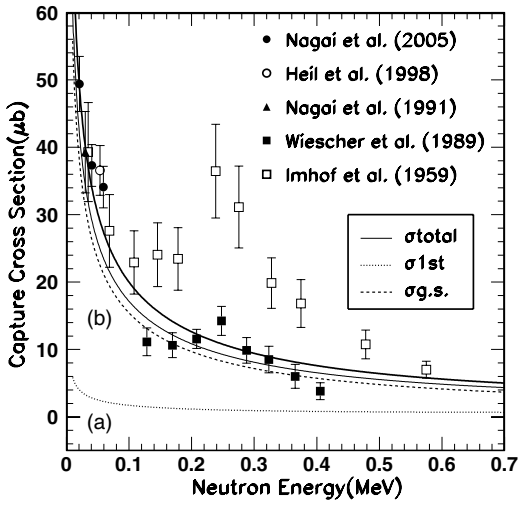

FIG. 6. The cross sections for the ^{7}Li(n,γ)^{8}Li capture reaction. The experimental points are from Refs. [12] and [30–33]. The curve labeled (a) (dotted line) is the sum of channel-spin $s = 1$ and $s = 2$ contributions for the neutron capture reaction to the first excited state of ^{8}Li, while curve (b) (dashed line) is the sum of the channel-spin $s = 1$ and $s = 2$ contributions for the ^{8}Li g.s. The thin solid line is the sum of these two contributions, where only the contribution of neutrons captured to the orbital $p_{3/2}$ in ^{8}Li(gs), using the spectroscopic factor $S_{^8\text{Li}}(\text{gs})(3/2) = 0.87$, is considered. The thick solid line is the same calculation considering in addition the contribution of the capture to the orbital $p_{1/2}$, using the spectroscopic factor $S_{^8\text{Li}}(\text{gs})(1/2) = 0.113$.

B. The ^{8}Li(n,γ)^{9}Li capture reaction

As mentioned above, the radiative neutron capture cross section for the ^{8}Li(n,γ)$^9\text{Li}_{\text{gs}}$ reaction cannot be obtained from a direct measurement. We here use the same prescription, based on a potential model, that was followed to calculate the cross section for the ^{7}Li(n,γ)^{8}Li reaction. The capture cross sections were calculated assuming that the ^{8}Li(n,γ)$^9\text{Li}_{\text{gs}}$ reaction proceeds by direct $E1$ capture of an s-wave neutron by $^8\text{Li}(J^\pi = 2^+)$ leading to the $^9\text{Li}(J^\pi = 3/2^-)$ g.s. The optical model potential used to generate the distorted wave for neutron scattering on the unstable ^{8}Li nucleus cannot be obtained experimentally. Instead, we used the same volume integral per nucleon as that of the n-^{7}Li potentials. Experimental optical model parameters can vary strongly for different systems, but the volume integral per nucleon of a potential is known to have less ambiguity and thus it can be considered a more stable quantity as a function of the masses of the interacting nuclei [26,34,35]. Thus, by scaling the real depth of the two entrance-channel spin components, $s = 1$ and $s = 2$, from the known n-^{7}Li potential in the previous analysis, and keeping the same volume integrals of the potential per nucleon ($J_V/A = 793$ MeV fm^3 and $J_V/A = 657$ MeV fm^3, respectively), $V_0 = 58.15$ MeV and $V_0 = 48.15$ are obtained for the depths of the potential wells for the two channel-spins ($s = 5/2$ and $s = 3/2$, respectively) of the n($1/2^+$)+$^8\text{Li}(2^+)$ system. To calculate the overlap integral of the $^8\text{Li} \otimes \text{n} = {}^9\text{Li}_{\text{gs}}$ bound system, a Woods-Saxon shaped potential is also considered. A depth $V_0 = 47.82$ MeV was obtained for potential by adjusting it to reproduce the binding energy ($E =$ 4.064 MeV). The normalization of this overlap integral is giving by the spectroscopic factor $S_{^9\text{Li}}(\text{gs}) = 0.62(7)$ extracted from the present analysis of the ^{9}Be(^{8}Li,^{9}Li)^{8}Be transfer reaction. With these potentials and the spectroscopic factor, the cross sections for the nonresonant part of the s-wave neutron capture reaction were calculated as a function of relative energy for both channel spins. The results of these calculations are shown in Fig. 7. The curve labeled (a) corresponds to the sum of the contribution of channel-spin $s = 3/2$ and $s = 5/2$, where each contribution was calculated with different scattering potential. The curves labelled (b) correspond to a different assumption for the scattering potential in which the

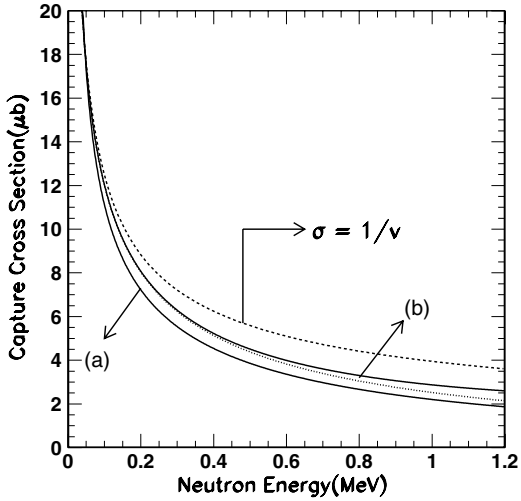

FIG. 7. The results of the capture cross section calculations for the ^{8}Li(n,γ)^{9}Li$_{gs}$ reaction. The lower curves labeled (a) correspond to the sum of channel-spin $s = 3/2$ and $s = 5/2$ assuming potential depths scaled from the n+^{7}Li capture reaction analysis, as explained in the text. Curves labeled (b) correspond to the assumption of same potential for the incoming wave function as for the bound state, for s-wave neutron only (dotted curve) and s- and d-wave neutrons (solid curve). The uppermost curve (dashed line) corresponds to a $1/v$ fit to the low-energy cross sections.

well depths are the same as that for the bound state. The dotted curve is obtained considering only an s-wave neutron, and the solid line is the sum of the s- and d-wave contributions. As one can see in Fig. 7, the onset of the higher partial wave component is observable only at higher energies.

To compare our results for the ^{8}Li(n,γ)^{9}Li$_{gs}$ capture reaction with other measurements and calculations, we have computed the nucleosynthesis reaction rate. The expression for the reaction rate for $E1$ capture in cm^3 mol^{-1} s^{-1} is given by [36]

$$N_A\langle\sigma v\rangle = K\int_0^\infty \sigma(E)E\exp(-C_2E/T_9)\,dE, \qquad (3)$$

where

$$K = C_1\mu^{-1/2}T_9^{-3/2}$$

and $C_1 = 3.7313\times10^{10}$, $C_2 = 11.605$, N_A is Avogadro's number, μ is the reduced mass of the system, T_9 is the temperature in units of 10^9 K, σ is the capture cross section, v is the relative velocity, and E is the energy in the center-of-mass system. E is given in MeV and the cross section is given in barns.

The reaction rate for the ^{8}Li(n,γ)^{9}Li$_{gs}$ capture reaction was estimated at a temperature $T_9 = 1$ and the integral of the expression [3] was performed up to 1.2 MeV. At this temperature, the capture reaction becomes important for the synthesis of heavier elements in the inhomogeneous Big Bang model. Also, the role of light neutron-rich nuclei for the r-process in Type II supernovae seems to be important at temperatures $0.5 < T_9 < 4$ [8]. Although the resonant

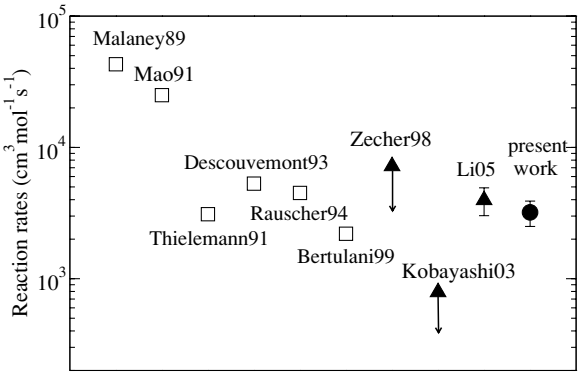

FIG. 8. Reaction rate for the direct neutron capture reaction ^{8}Li(n,γ)^{9}Li$_{gs}$ calculated at $T_9 = 1$. The open squares are calculations from Refs. [37–42] and the solid triangles are experimental estimations from Refs. [9,26], and [43].

capture through the $\frac{5}{2}^-$ resonance in ^{9}Li could be important for temperatures higher than $T_9 = 0.5$, in the present calculation only the direct capture to ^{9}Li at the g.s. is considered.

At energies up to 1 MeV, the capture reaction is completely dominated by s-wave neutrons. The contribution of the d-wave neutron to the reaction rate is estimated to be less than 0.5% at these energies and it becomes important only at high energies. Assuming a distorted wave from the potentials that have the same volume integral per nucleon as for the n+^{7}Li system, the reaction rate for the ^{8}Li(n,γ)^{9}Li$_{gs}$ capture reaction was deduced to be $N_A\langle\sigma v\rangle = (3.17\pm0.70)\times 10^3$ cm^3 mol^{-1} s^{-1}, where the uncertainty is from the uncertainty in the spectroscopic factor used in the calculation (20%) and from the variation of ±1 MeV in the potentials used to determined the distorted wave (10%). As suggested by Mengoni *et al.* [11], a different assumption would be to use the same potential for the incoming channel as that used for the bound state. With this assumption for the n-^{8}Li potential, the reaction rate is determined to be $N_A\langle\sigma v\rangle = (3.23\pm0.71)\times 10^3$ cm^3 mol^{-1} s^{-1}. The average value adopted here is

$$N_A\langle\sigma v\rangle = (3.20\pm0.70)\times10^3 \text{ cm}^3 \text{ mol}^{-1} \text{ s}^{-1}.$$

In Fig. 8, this value is compared with theoretical calculations reported in Refs. [37–42] and experimental estimations from Refs. [9,43], and [26]. Our result is comparable to the most recent theoretical calculations [39–42] and is in good agreement with the value from a recent (d,p) experiment [26]. The small difference obtained in the reaction rate between these two experiments can be attributed in part to the different approaches used in the calculation of the neutron scattering potential. Both results are significantly higher than the upper limit obtained in the most recent Coulomb dissociation experiment by Kobayashi *et al.* [9].

A $1/v$ behavior of the capture cross section as a function of relative energy is expected for s-wave neutron capture at low energies. However, as can be seen in Fig. 7, the reaction rate obtained in the potential model follows a $1/v$ dependence

only for very low energies ($E_n < 0.1$ MeV). Normalizing a $1/v$ curve to the values given by the potential model in the energy range from 0 to 0.1 MeV, the corresponding expression for the capture cross section becomes

$$\sigma(n,\gamma) = 3.95 \times E_n^{-1/2},$$

where E_n is the neutron energy in MeV and $\sigma(n,\gamma)$ is given in μb. The corresponding reaction rate integrated over the range up to 1.2 MeV (which would be in this case energy independent) is

$$N_A\langle\sigma v\rangle = 3.27 \times 10^3 \text{ cm}^3 \text{ mol}^{-1} \text{ s}^{-1},$$

which is in agreement with the value obtained directly from the potential model and also much higher than the upper limit obtained by Kobayashi *et al*. [9].

Pandharipande [44] has argued that absolute spectroscopic factors (SF) obtained from nucleon transfer reactions are model dependent and may be systematically too high by as much as 60%, due to the fact that these reactions probe only the asymptotic region of the overlap integrals. This criticism would apply equally to the SF extracted from the (d,p) reaction in Ref. [26]. As a result, the reaction rates from both experiments might have to be multiplied by a factor of 0.65, bringing them into somewhat better agreement with the upper limit quoted in Ref. [9]. However, a recent extensive survey of neutron spectroscopic factors by Tsang, Lee, and Lynch [45] indicated a good overall agreement between measured relative SF from (d,p) and (p,d) reactions and large basis shell model calculations. In the present case, we have shown that the absolute value of the ^{7}Li + n reaction rate is well-reproduced using the techniques employed here. As a result, the corresponding ^{8}Li + n reaction rate is not expected to be affected by these considerations except in the unlikely event that the ^{8}Li mean-field potential is very different from that of ^{7}Li.

V. SUMMARY

We measured the angular distributions for the elastic scattering of ^{8}Li on ^{9}Be and the neutron transfer reactions ^{9}Be(^{8}Li,^{7}Li)^{10}Be and ^{9}Be(^{8}Li,^{9}Li)^{8}Be at $E_{LAB} = 27.0$ MeV. Spectroscopic factors for the $^8\text{Li}_{gs} \otimes \text{n} = {}^9\text{Li}_{gs}$ and $^7\text{Li}_{gs} \otimes \text{n} = {}^8\text{Li}_{gs}$ bound systems were obtained from the comparison between the experimental differential cross sections and FR-DWBA calculations with the code FRESCO. The spectroscopic factors obtained were compared with shell model calculations and also with experimental values from (d,p) reactions. Using the spectroscopic factors extracted from the angular distributions for the $^8\text{Li}_{gs} \otimes \text{n} = {}^9\text{Li}_{gs}$ and $^7\text{Li}_{gs} \otimes \text{n} = {}^8\text{Li}_{gs}$ bound system, we derived the cross-sections for the ^{7}Li(n,γ)^{8}Li and ^{8}Li(n,γ)$^9\text{Li}_{gs}$ neutron capture reactions based on a potential model. The reaction rates for the nonresonant part of the ^{8}Li(n,γ)$^9\text{Li}_{gs}$ reaction were compared with the results from previous indirect methods and with theoretical calculations. Our work has shown that low-energy radioactive nuclear beams can be very suitable not only to perform spectroscopic investigations but also to determine the nonresonant parts of capture reactions of astrophysics interest.

ACKNOWLEDGMENTS

The authors thank the Fundação de Amparo a Pesquisa do Estado de São Paulo (FAPESP 2001/06676-9 and 2006/00629-2) for financial support. This work was also funded in part by the U.S. NSF under Grants PHY03-54828 and INT03-05347.

[1] I. J. Thompson, Comput. Phys. Rep. **7**, 167 (1988), and www.fresco.org.uk.
[2] T. Nakamura *et al*., Phys. Rev. Lett. **96**, 252502 (2006).
[3] N. Michel, W. Nazarewicz, M. Ploszajczak, and J. Rotureau, Eur. J. Phys. A **25**, 493 (2005).
[4] P. Navratil, Phys. Rev. C **70**, 054324 (2004).
[5] P. Santi *et al*., Phys. Rev. C **67**, 024606 (2003).
[6] T. Kajino and R. N. Boyd, Astrophys. J. **359**, 267 (1990).
[7] J. Gorres, H. Herndl, I. J. Thompson, and M. Wiescher, Phys. Rev. C **52**, 2231 (1995).
[8] M. Terasawa, K. Sumiyoshi, T. Kajino, G. J. Mathews, and I. Tanihata, Astrophys. J. **562**, 470 (2001).
[9] H. Kobayashi *et al*., Phys. Rev. C **67**, 015806 (2003).
[10] C. A. Gagliardi, A. Azhari, V. Burjan, F. Carstoiu, V. Kroha, A. M. Mukhamedzhanov, A. Sattarov, X. Tang, L. Trache, and R. E. Tribble, Eur. Phys. J. A **13**, 227 (2002).
[11] A. Mengoni, T. Otsuka, and M. Ishihara, Phys. Rev. C **52**, R2334 (1995).
[12] Y. Nagai, M. Igashira, T. Takaoka, T. Kikuchi, T. Shima, A. Tomyo, A. Mengoni, and T. Otsuka, Phys. Rev. C **71**, 055803 (2005).
[13] M. Assunção, R. Lichtenthaler, V. Guimarães, A. Lepine-Szily, G. F. Lima, and A. M. Moro, Phys. Rev. C **70**, 054601 (2004).
[14] K. W. Kemper, G. E. Moore, R. J. Puigh, and R. L. White, Phys. Rev. C **15**, 1726 (1977).
[15] J. Cook and K. W. Kemper, Phys. Rev. C **31**, 1745 (1985).
[16] F. D. Becchetti *et al*., Nucl. Instrum. Methods Res. A **505**, 377 (2003).
[17] G. E. Knoll, *Radiation Detection and Measurement* (Wiley & Sons, New York, 1989), p. 380.
[18] C. M. Perey and F. G. Perey At. Data Nucl. Data Tables **17**, 1 (1976).
[19] L. C. Chamon, B. V. Carlson, L. R. Gasques, D. Pereira, C. De Conti, M. A. G. Alvarez, M. S. Hussein, M. A. Candido Ribeiro, E. S. Rossi, Jr., and C. P. Silva, Phys. Rev. C **66**, 014610 (2002).
[20] L. Trache, A. Azhari, F. Carstoiu, H. L. Clark, C. A. Gagliardi, Y.-W. Lui, A. M. Mukhamedzhanov, X. Tang, N. Timofeyuk, and R. E. Tribble, Phys. Rev. C **67**, 062801(R) (2003).
[21] D. L. Powell, G. M. Grawley, B. V. N. Rao, and B. A. Robson, Nucl. Phys. **A147**, 65 (1970).
[22] S. E. Darden, G. Murillo, and S. Sen, Nucl. Phys. **A266**, 29 (1976).
[23] S. Cohen and D. Kurath, Nucl. Phys. **A101**, 1 (1967).
[24] P. Mohr, Phys. Rev. C **67**, 065802 (2003).
[25] W. Fitz, R. Jahr, and R. Santo, Nucl. Phys. **A101**, 449 (1967).

[26] Z. H. Li, W. P. Liu, X. X. Bai, B. Guo, G. Lian, S. Q. Yan, B. X. Wang, S. Zeng, Y. Lu, J. Su, Y. S. Chen, K. S. Wu, N. C. Shu, and T. Kajino, Phys. Rev. C **71**, 052801(R) (2005).
[27] H. B. Jeppesen *et al*., Phys. Lett. **B635**, 17 (2006).
[28] A. H. Wuosmaa *et al*., Phys. Rev. Lett. **94**, 082502 (2005).
[29] C. A. Bertulani, Comput. Phys. Commun. **156**, 123 (2003).
[30] M. Heil, F. Kaeppeler, M. Wiescher, and A. Mengoni, Astrophys. J. **507**, 997 (1998).
[31] Y. Nagai, M. Igashira, N. Mukai, T. Ohsaki, F. Uesawa, K. Takeda, T. Ando, H. Kitazawa, S. Kubono, and T. Fukuda, Astrophys. J. **381**, 444 (1991).
[32] M. Wiescher, R. Steininger, and F. Kappeler, Astrophys. J. **344**, 464 (1989).
[33] W. L. Imhof *et al*., Phys. Rev. **114**, 1037 (1959).
[34] G. R. Satchler, *Nuclear Reactions*, 2nd ed. (Oxford University Press, New York, 1990), p. 192.
[35] F. D. Becchetti and G. W. Greenlees, Phys. Rev. **182**, 1190 (1969).
[36] C. Angulo *et al*., Nucl. Phys. **A656**, 3 (1999).
[37] R. A. Malaney and W. A. Fowler, Astrophys. J. **345**, L5 (1989).
[38] Z. Q. Mao and A. E. Champagne, Nucl. Phys. **A522**, 568 (1991).
[39] F. K. Thielemann, J. H. Applegate, J. H. Cowan, and M. Wiescher, in *Nuclei in the Cosmos, Baden, Viena 1990*, edited by H. Oberhummer (Springer-Verlag, Heildelberg, 1991), p. 147.
[40] P. Descouvemont, Astrophys. J. Lett. **405**, 518 (1993).
[41] T. Rauscher, J. H. Applegate, J. J. Cowan, F. K. Thielemann, and M. Wiescher, Astrophys. J. **429**, 499 (1994).
[42] C. A. Bertulani, J. Phys. G **25**, 1959 (1999).
[43] P. D. Zecher *et al*., Phys. Rev. C **57**, 959 (1998).
[44] V. Pandharipande, Rev. Mod. Phys. **69**, 981 (1997).
[45] M. B. Tsang, J. Lee, and W. G. Lynch, Phys. Rev. Lett. **95**, 222501 (2005).